

## DETERMINATION OF THE RESONANCE FREQUENCIES OF THE MAGNETIC NEAR-FIELD RADIATED BY A SMPS

**C. Labarre** <sup>†</sup>

Université Lille Nord de France  
Lille F 59000, France

**F. Costa** <sup>‡</sup>

SATIE (UMR 8029), ENS de Cachan PRES UniverSud  
61 av. du président Wilson, Cachan 94235, France

**J. Ecrabey**

Schneider Electric  
Grenoble F-38050, France

**Abstract**—In this paper, we analyze the behaviour of a switched mode power supply (SMPS) regarding the radiated magnetic near-field through an initial understanding of the electrical working of the converter, particularly during switchings. We propose a method based on impedance analysis at each state of the converter in order to predict the resonances of currents and/or voltages in the SMPS at the origin of the magnetic radiated near-field.

### 1. INTRODUCTION

Measurement techniques that are usually used for the characterization of radiated and conducted emissions of power electronics are mainly concerned by the compliance with EMC standards. Actually, near-field techniques constitute also an efficient approach to characterize complex radiating systems [1, 2]. From near-field scannings, equivalent

---

*Received 7 December 2010, Accepted 21 January 2011, Scheduled 27 January 2011*

Corresponding author: Cecile Labarre (cecile.labarre@mines-douai.fr).

<sup>†</sup> Also with EM Douai, Douai IA F 59508, France.

<sup>‡</sup> Also with IUFM de Créteil, Université Paris Est Créteil place du 8 mai 1945, Saint-Denis 93000, France.

models can be deduced for representing electromagnetic emissions [3–5]. However, near-field scanning over a power electronic device is not referenced in standards, but it can be useful to estimate the characteristics of radiations and to locate spatially the sources of electromagnetic fields [6]. Due to their working principle, switching-mode power supplies (SMPS) are disturbing subsystems. Many papers [7, 8] propose the modeling and the prediction of conducted electromagnetic interferences (EMI) in SMPS but few [9, 10] deal with the modeling and the prediction of radiated near-field emissions. The objective of our paper is to predict the resonance frequencies of the radiated magnetic near-field. In the SMPS studied, several radiating sources were identified: the switching cell of the SMPS at the input stage, the snubbers and the transformer due to its imperfections (fringing flux, parasitic capacitances). First, based on the modelling of the SMPS, the correlation between the disturbances emitted in magnetic near-field and the electric working of the SMPS is established. In a second step, the resonance frequencies will be predicted according to the different working steps of the converter variables. This step can help designers to satisfy EMI regulations at lowest cost and to cope with EMI problems easily before manufacturing.

## 2. FLYBACK CONVERTER DESCRIPTION

The SMPS considered in this paper is a part of an industrial variable speed drive (VSD); it was identified as an important disturbing source in this equipment [11]. It contains a transformer, made up of a double primary and seven secondary windings. In most cases of working of the VSD, only a single winding transmits power. Then, the study was reduced by considering that the transformer was only made of the two used windings, as it is shown in the electric schema of Figure 1. The currents which flow in the transformer are divided into two categories: the differential mode ones flowing in the windings and the common mode ones flowing between the floating voltage of the transistor and the frame and inside the parasitic elements of the component as represented in Figure 1. This paper is focussed on the differential mode currents because our preliminary investigations showed that they are mainly responsible for the magnetic near-field radiation. Firstly, the heat-sink and the secondary winding aren't connected to ground. In Figure 1, we drew  $C_{ph}$  the parasitic capacitance between the heat-sink and ground and  $C_{pl}$  the parasitic capacitance between the secondary winding and ground. These low parasitic capacitances (some pF) lead to a high common mode impedance, that limits the common mode current flowing. Secondly, due to an optimized layout, the surfaces

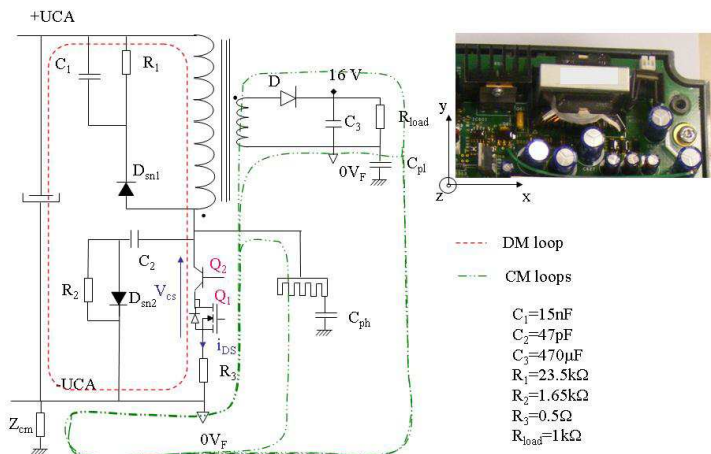


**Figure 1.** Reduced SMPS electric schema.

of the common mode loops are reduced. So, their contribution to the magnetic field is reduced too. This is the reason why we modeled only, the main differential loop, which is constituted by the switch, the snubbers and the transformer [12].

### 3. MODELLING OF THE DIFFERENTIAL MODE LOOP

Before presenting the complete SMPS modelling, the modelling of the transformer is presented hereinafter.

#### 3.1. Transformer Modelling

In order to take into account the complete (magnetic and electrostatic) behavior of the transformer, a model with three capacitances [13, 14], is used. It is represented in Figure 2. The series resistance,  $R_s$ , is the one of the copper winding. The series inductance,  $L_f$ , models the flux leakage. The parallel resistance,  $R_f$ , represents the core loss of the magnetic material due to hysteresis and eddy currents. The parallel inductance,  $L_\mu$ , called the magnetizing inductance, accounts for the finite permeability of the magnetic core.  $C_{pp}$ , respectively  $C_{ps}$ , is the parasitic capacitance of the primary, respectively secondary, winding.  $C_p$  is the parasitic capacitance between the primary and secondary windings.  $m$  is the transformer ratio.

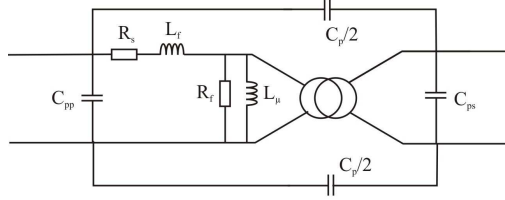


**Figure 2.** The electromagnetic model of a transformer with two windings.

The transformer is modeled by a two-port, characterized by its admittance matrix  $[Y]$  such as:

$$[Y] = \begin{pmatrix} Y_{11} & Y_{12} \\ Y_{21} & Y_{22} \end{pmatrix} \quad (1)$$

with

$$Y_{11} = j\omega(C_p + C_{pp}) + \frac{1}{R_s + jL_f\omega} \quad (2)$$

$$Y_{12} = Y_{21} = j\omega C_p - \frac{1}{m(R_s + jL_f\omega)} \quad (3)$$

$$Y_{22} = j\omega(C_p + C_{pp}) + \frac{1}{m^2} \left( \frac{1}{R_s + jL_f\omega} + \frac{1}{R_f} + \frac{1}{jL_\mu\omega} \right) \quad (4)$$

The parallel parameter values  $L_\mu$  and  $R_f$  are found with no load connected to the secondary (open circuit) and the series parameter values  $R_s$  and  $L_f$  are found with the secondary terminals shorted (short-circuit).  $C_p$  is measured by shorting the primary and secondary windings to themselves and connecting them to the inputs of a network analyzer.  $C_{pp}$  and  $C_{ps}$  can't be determined experimentally. The input impedance of the transformer with the secondary winding open or short-circuited can be deduced from (1). By fitting this model of impedance with the corresponding measurements, the two missing values are determined. All the parameters are given in Table 1.

In Figure 3, for the configuration where the secondary winding is open-circuited, we compare the measured input impedance modulus with the one calculated by the model. The good accordance between the two curves shows that our model is valid roughly up to 7 MHz, which is sufficient for analysis regarding the frequency range of magnetic near-field radiations. Over this frequency the influence of the other windings is important and requires to improve the model.

### 3.2. Flyback Converter Complete Modelling

The complete SMPS model including the transformer is represented by the equivalent electric circuit of Figure 4.  $E$  is the DC source.  $Z_L$  is the load impedance, it's the parallel combination of  $R_{load}$  and  $C_3$ . The two transistors of the switching cell were replaced by an equivalent ideal switch  $K$  [15].  $C_k$  is the parasitic capacitance of the equivalent switch ( $Q_1$  and  $Q_2$ ).  $C_D$  is the parasitic capacitance of the secondary diode  $D$ .  $L_p$  is the parasitic inductance of the PCB tracks and the connections of the transistor.  $C_{sn1}$ , respectively  $C_{sn2}$  is the parasitic capacitance of  $D_{sn1}$ , respectively  $D_{sn2}$ .

**Table 1.** Electrical model parameters.

Parameters	Value
$C_{pp}$	20 pF
$C_{ps}$	1200 pF
$C_p$	15 pF
$L_\mu$	0.42 mH
$L_f$	28 $\mu$ H
$R_s$	4 $\Omega$
$R_f$	100 k $\Omega$
$m$	0.19

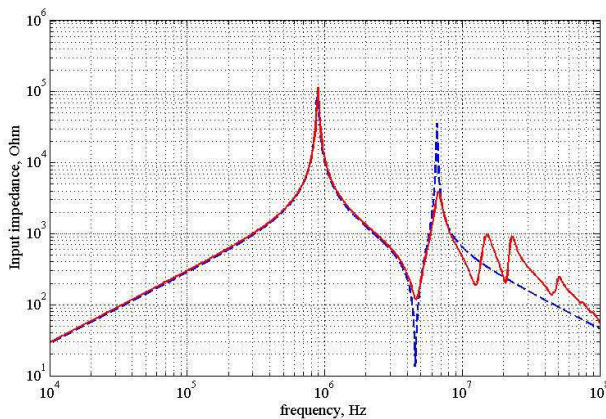


**Figure 3.** Comparison between the modeled (dashed line) and measured (solid line) input impedances for open circuit load.

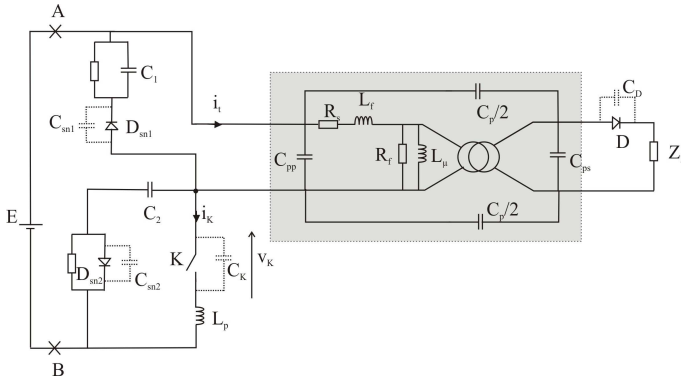


**Figure 4.** Equivalent electrical scheme of the flyback converter.

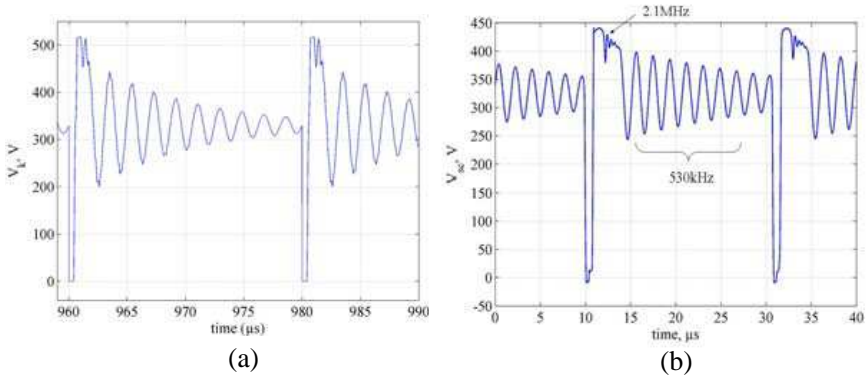


**Figure 5.** (a) Simulated voltage  $V_k$ . (b) Measured voltage  $V_{cs}$ .

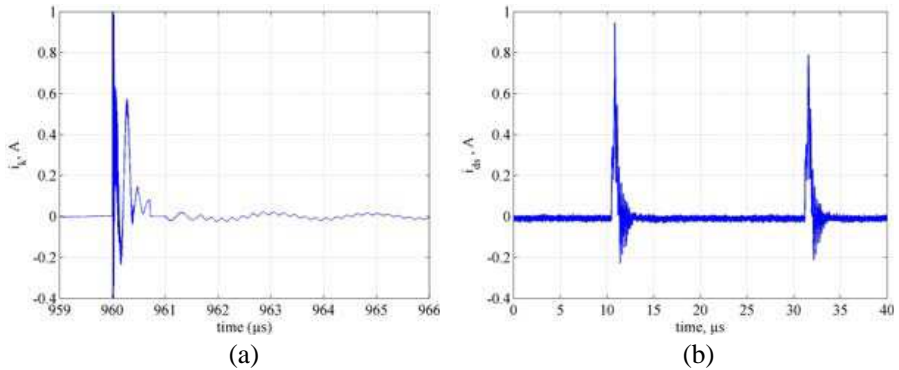


**Figure 6.** (a) Simulated current  $i_k$ . (b) Measured current  $i_{ds}$ .

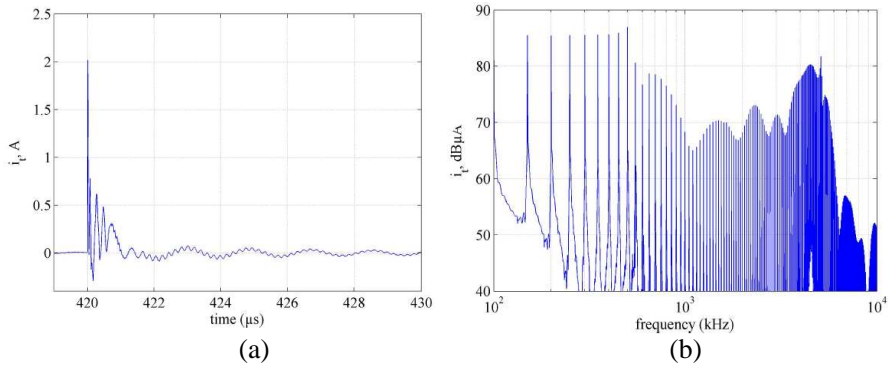


**Figure 7.** (a) Simulated current  $i_t$ . (b) Simulated amplitude spectrum of current  $i_t$ .

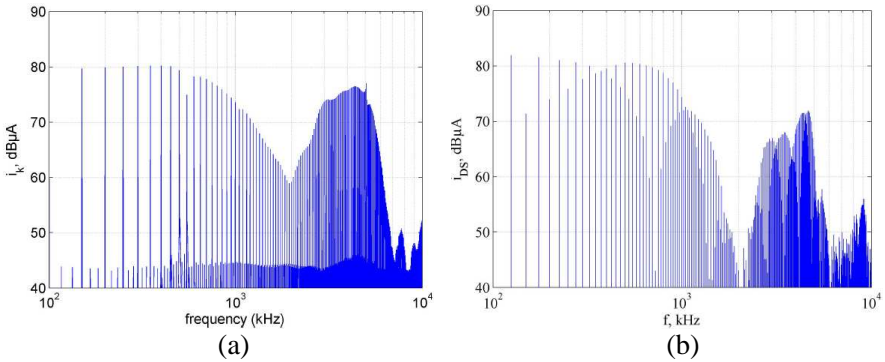


**Figure 8.** (a) Simulated amplitude spectrum of current  $i_k$ . (b) FFT-computed amplitude spectrum of measured current  $i_{ds}$ .

In order to validate our model, this electrical circuit (Figure 4) was simulated with PSIM® simulation software. The simulated currents and voltage are indicated in Figure 4. In Figure 5(a), we observe two resonance frequencies at 509 kHz and 2.34 MHz in the voltage  $v_k$ . In Figure 6(a), we notice a resonance frequency at 4.57 MHz and an HF oscillation in the current  $i_k$ . In Figure 7(a), we observe the same resonance frequency at 4.57 MHz in the current  $i_t$ . The spectra of currents  $i_k$  and  $i_t$  were also computed with PSIM®, they are presented in Figures 8(a) and 7(b).

#### 4. ELECTRICAL ANALYSIS

The key waveforms of the SMPS were measured: the voltage  $V_{cs}$  at the boundaries of the equivalent switch ( $Q_1$  and  $Q_2$ ) and the current  $i_{ds}$ . Since the device under test is an industrial device, it wasn't easy to make electrical measurements and it wasn't possible to measure current  $i_t$  in the transformer. The measurement points of the voltage  $V_{cs}$  and the current  $i_{ds}$  are shown in Figure 1. Current  $i_{ds}$  is measured indirectly; it is deduced from a voltage measurement.

These measurements are shown in Figures 5(b) and 6(b). The current measurement was achieved at a different time scale in order to identify the resonance frequencies (Figure 9).

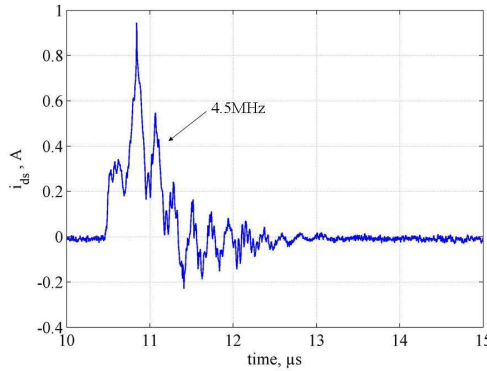


**Figure 9.** Measured current  $i_{ds}$  at a different time scale.

We can notice that each current switching is accompanied by two damped oscillations at 4.5 MHz. Voltage  $V_{cs}$  exhibits also two resonance frequencies at 530 kHz, when both transistor and diode are switched-off, and at 2.1 MHz. These frequencies correspond satisfactorily to the ones found by simulation (509 kHz, 2.34 MHz and 4.57 MHz) in Section 3. The HF oscillation observed in the simulated current doesn't appear in the measured current, due to the probe bandwidth.

To complete our investigations, the spectrum of current  $i_{ds}$  was computed by FFT, it is presented in Figure 8(b). It is also in a good accordance with the spectrum of the simulated current  $i_k$  shown in Figure 8(a). That allows to validate our equivalent electrical model.

## 5. NEAR-FIELD MEASUREMENTS

### 5.1. Magnetic Field Spectrum Measurement

At a distance of 7 centimeters on the vertical axis of the transformer, in the band [100 kHz–10 MHz], the magnetic near-field radiated by the SMPS working alone (the VSD inverter isn't working) was measured. The magnetic field spectrum of the component  $H_z$ , perpendicular to the plane of the VSD, is shown in Figure 10.

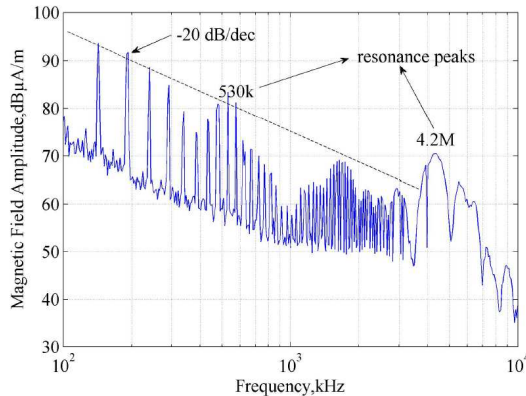


**Figure 10.** Measured magnetic field  $z$ -component spectrum.

In the range of frequency, that extends from 100 kHz to 1 MHz, the peaks with decreasing amplitudes by  $-20$  dB/dec are the harmonics multiple of the switching frequency (50 kHz). However, over this tendency, larger peaks appear at particular frequencies as shown in Figure 10. In the range that extends roughly from 1 MHz to 20 MHz, the phenomena linked to the switching transients appear and lead to resonances. They depend on the intrinsic parasitic elements of the switches, their driving speed and the parasitic elements associated to the transformer windings. This spectrum can be compared with the simulated amplitude spectrum of current  $i_t$  (Figure 7(b)) which confirms that the current flowing in the primary winding of the transformer produces mainly the magnetic field. If we consider the spectrum envelope, significant peaks appear around 530 kHz and 4.2 MHz, frequencies already identified. To complete this measurement, near-field scannings were achieved with our test bench, which will be described shortly in the following paragraph.

## 5.2. The Near-field Measurement System

A three-dimensional near-field scanner is used to measure the magnitude of the magnetic near-field in a plane at a specific height above a power electronic device. The equipment is rated to work in a bandwidth situated between 9 kHz and 1 GHz. The measurements of the three components of the magnetic field are achieved with  $H$  field probes (AFJ near-field probe, set LF1). They consist of small electrically balanced loop antennas. These loop probes measure the magnetic field perpendicular to the loop. The three components of the magnetic field are obtained by rotating the probe with an angle of  $90^\circ$  around the three  $x$ ,  $y$  and  $z$  directions. In order to reduce measurements time, a data post-processing based on the Wiener filtering [16] is applied.

## 5.3. Near-field Scanning Results

$H$ -field scanings parallel to the plane of the VSD were achieved. Figure 11 shows the  $z$ -component of the magnetic near-field at 530 kHz and at 4.2 MHz, the two significant resonance frequencies. At 530 kHz, the magnetic near-field is essentially located over the transformer whereas at the other frequency, the magnetic near-field is located over the transformer but it is also scattered by the EMI filter and by the output connections of the SMPS. These measurements show clearly that the main source of radiated  $H$ -field is the transformer and its

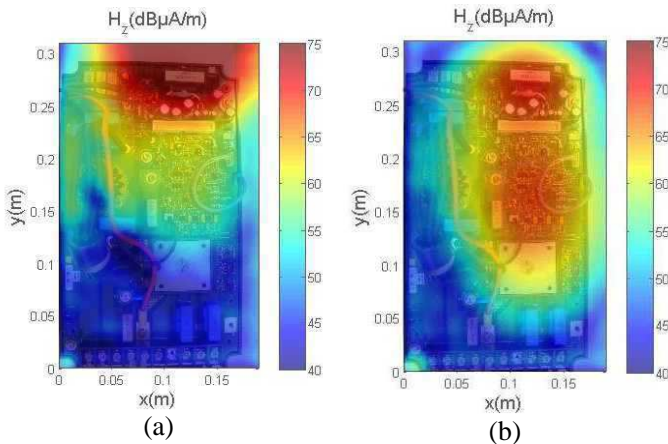


**Figure 11.** Scanning of the  $z$ -component of the magnetic near-field. (a) @ 530 kHz. (b) @ 4.2 MHz.

**Table 2.** Definition of the switches states for each working phase.

Phase	$K$	$D_{sn2}$	$D_{sn1}$	$D$	Duration ( $\mu\text{s}$ )	Resonance frequencies
1	1	0	0	0	0.75	4.5 MHz
2	0	1	0	0	0.25	470 kHz, 4.9 MHz
3a	0	1	0	1	0.05	2 MHz
3b	0	0	1	1	0.8	none
4	0	0	0	1	2.1	2.1 MHz
5	0	0	0	0	16.6	490 kHz, 5 MHz

fringing flux. The other loops radiate at a lower order of magnitude; this is due to the very compact layout of the converter which limits the leakage flux only to the transformer. Their influence are quite undetectable on these scannings, except at 4.2 MHz. However, the understanding of the causes of these ringings is of importance.

## 6. KEY WAVEFORMS AND IMPEDANCE ANALYSIS

The various switching states of the converter are defined in Table 2. Their duration deduced from current and voltage measurements are precise. In Figure 12, the theoretical waveforms corresponding to these different working phases are presented. The switching changes the initial conditions of resonant circuits in the SMPS, leading to ringings with low damping. The resonance frequencies corresponding to a maximal radiated magnetic field correspond also to a maximal differential mode current, at the origin of the magnetic near-field. So, the resonance frequencies can be found by impedance analysis for each state of the SMPS switches. For each working phase, an electric circuit of the input of the SMPS can be drawn from the general equivalent electric diagram of Figure 4. The equivalent input impedance seen from the voltage source  $E$  of the SMPS  $Z_{AB}$  can be calculated. As  $E$  is a constant voltage source, the zeros of the impedance modulus  $Z_{AB}$  correspond to a maximal differential mode current, and then to a maximal radiated magnetic near-field. This is the reason why only the zeros of  $Z_{AB}$  are used to identify the resonance modes in the different working phases. So, the successive analyses can be done.

- In phase 1, switch  $K$  is turned on. All the other switches are turned off. In Figure 13(a), we can notice a resonance frequency of the impedance  $Z_{AB}$  at 4.5 MHz.
- In phase 2, when switch  $K$  is turned off quickly, the primary current  $i_k$  charges  $C_k$  in a short time. The voltage  $V_k$  across

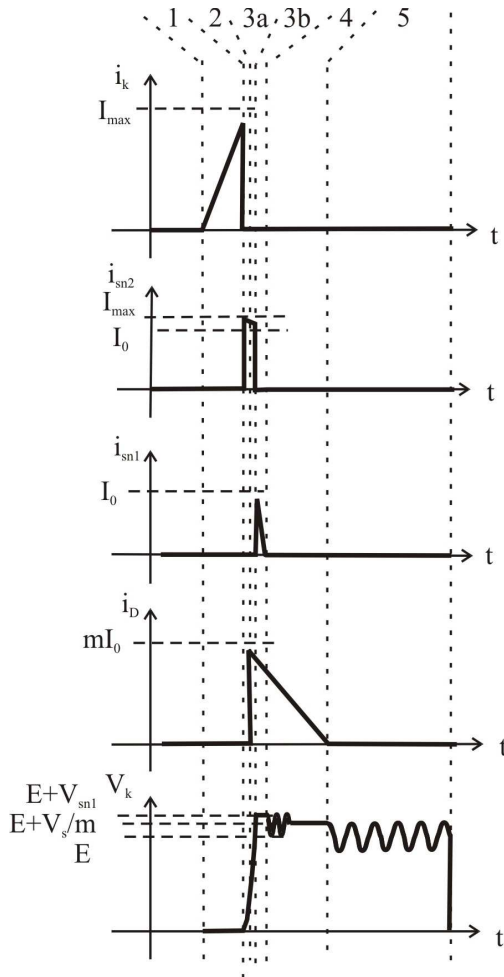


**Figure 12.** Key waveforms of the Flyback converter.

$C_k$  increases. Diode  $D_{sn2}$  (turn-off snubber) is turned on and capacitor  $C_2$  is being charged.

- In phase 3a, when  $V_k$  exceeds  $E + \frac{V_s}{m}$ , with  $\frac{V_s}{m}$  the reflected output voltage, the secondary diode  $D$  turns on.
- In phase 3b, the RCD snubber circuit absorbs the current in the leakage inductor by turning on the snubber diode  $D_{sn1}$  when voltage  $V_k$  reaches  $E + V_{sn1}$ . The primary current flows to  $C_{sn1}$  through the snubber diode  $D_{sn1}$ , voltage  $V_{sn1}$  across the snubber capacitor  $C_{sn1}$  increases in a small amount. This phase ends when

the leakage energy stored in  $L_f$  is fully dissipated in the RCD snubber, that is  $i_{sn1}$  is null.

The phases 2, 3a and 3b are very short times.

- In phase 4, when  $V_{cs}$  is equal to  $E + \frac{V_s}{m}$ , diode  $D_{sn1}$  transfers energy stored in  $L_\mu$  to the secondary circuit. This phase ends when  $i_D$  reaches 0.
- In phase 5, all the switches are turned off.

Figure 13(b) presents the impedance  $Z_{AB}$  in the phases 4 and 5. We can observe a resonance frequency at 2.1 MHz in phase 4 and two resonance frequencies (490 kHz and 5 MHz) in phase 5.

In phase 1, the resonance at 4.5 MHz can be observed in current  $i_{ds}$  (Figure 9) as well as in the spectrum of this current (Figure 8(b)) and in the magnetic near-field spectrum (Figure 10). Phase 2 and 3a are too short for oscillations to appear. During phases 4 and 5, the predicted resonance frequencies (2.1 MHz and 490 kHz) can be observed in voltage  $V_{cs}$  (Figure 5(b)). The first resonance frequency doesn't appear in current  $i_{ds}$  because it is hidden in the noise level but both can be observed in the magnetic near-field spectrum (Figure 10). The difference between the predicted resonance frequency (490 kHz) and the measured one (530 kHz) can be explained by the uncertainty of the  $C_k$  value. So, all resonance frequencies identified using this method can be observed in the current  $i_{ds}$  or voltage  $V_{cs}$  waveforms and consequently in the radiated near-field  $H$ .

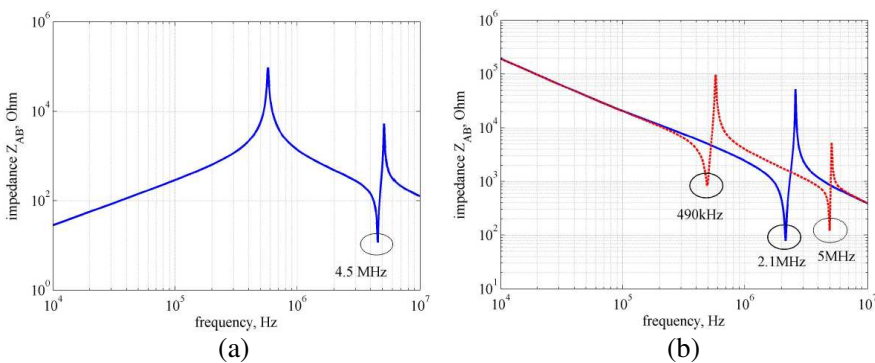


**Figure 13.** Input impedance of the SMPS enabling to determine the resonance. (a) Phase 1. (b) Phase 4 (solid line) and phase 5 (dashed line).

## 7. CONCLUSION

A process to correlate the magnetic near-field spectrum and the electric working of the SMPS of an industrial VSD has been developed. Considering that the switching changes the initial conditions of resonant circuits in the SMPS and leads to ringings, an equivalent circuit model including parasitic elements is established for each state of the SMPS switches and the resonance frequencies are determined by impedance analysis. All predicted resonance frequencies were observed in one of the electric quantities. Thanks to this analysis, it would be possible to modify the transformer building in order to avoid the most drastic resonances leading to severe radiated and conducted EMI or to optimize damping circuits.

## REFERENCES

1. Hernando, M., A. Fernandez, M. Arias, M. Rodriguez, Y. Alvarez, and F. Las-Heras, "Radiated noise measurement system to estimate the EMI regulations compliance of a power electronic system," *Proceedings ISIE*, Vigo, Spain, 2007.
2. Baudry, D., A. Louis, and B. Mazari, "Characterization of the open-ended coaxial probe used for near-field measurements in emc applications," *Progress In Electromagnetics Research*, Vol. 60, 311–333, 2006.
3. Vives-Gilabert, Y., C. Arcambal, A. Louis, F. de Daran, P. Eudeline, and B. Mazari, "Modeling magnetic radiations of electronic circuits using near-field scanning method," *IEEE Transactions on Electromagnetic Compatibility*, Vol. 49, No. 2, 391–400, May 2007.
4. Liu, B., L. Beghou, L. Pichon, and F. Costa, "Adaptive genetic algorithm based source identification with near-field scanning method," *Progress In Electromagnetic Research B*, Vol. 9, 215–230, 2008.
5. Tong, X., D. W. Thomas, A. Nothofer, P. Sewell, and C. Christopoulos, "Modeling electromagnetic emissions from printed circuit boards in closed environments using equivalent dipoles," *IEEE Transactions on Electromagnetic Compatibility*, Vol. 99, 1–9, 2010.
6. Chen, P. and Z. Qian, "The EMI design of low power isolated converter based on near field measure," *Proceedings Asia-Pacific Conference on Environmental Electromagnetics, CEEM 2003*, 407–409, Nov. 4–7, 2003.

7. Gonzalez, D., J. Gago, and J. Balcells, "New simplified method for the simulation of conducted EMI generated by switched power converters," *IEEE Transactions on Industrial Electronics*, Vol. 50, No. 6, 1078–1084, Dec. 2003.
8. Crebier, J.-C. and J.-P. Ferrieux, "PFC full bridge rectifiers EMI modeling and analysis-common mode disturbance reduction," *IEEE Transactions on Power Electronics*, Vol. 19, No. 2, 378–387, Mar. 2004.
9. Bai, F., Z.-X. Niu, Y.-J. Shi, and D.-F. Zhou, "Nearfield modeling and prediction of switched mode power supply," *IEEE Conference on Power Electronic, Drives and Energy Systems*, 2006.
10. Chen, W., L. Feng, H. Chen, and Z. Qian, "Near field coupling effects on conducted EMI in power converter," *37th IEEE Power Electronics Specialists Conference, PESC'06*, 1–6, Jun. 18–22, 2006.
11. Aouine, O., C. Labarre, F. Costa, and J. Ecrabey, "Modelling and analysis of the magnetic field radiated by a switching mode power supply," *35th Annual Conference of IEEE Industrial Electronics, IECON'09*, 4116–4121, Nov. 2009.
12. Meng, P., X. Wu, J. Yang, H. Chen, and Z. Qian, "Analysis and design considerations for EMI and losses of RCD snubber in flyback converter," *2010 Twenty-Fifth Annual IEEE Applied Power Electronics Conference and Exposition (APEC)*, 642–647, Feb. 21–25, 2010.
13. Mao, X. and W. Chen, "More precise model for parasitic capacitances in high-frequency transformer," *2002 IEEE 33rd Annual Power Electronics Specialists Conference, PESC 02*, Vol. 2, 1054–1057, 2002.
14. Tarateeraseth, V., T. Maneenopphon, and W. Khan-ngern, "The comparison of EMI and electrical performances of high frequency transformer windings for smps applications," *Power Conversion Conference — Nagoya, PCC'07*, 435–440, Apr. 2–5, 2007.
15. Mugur, P. R., J. Roudet, and J. C. Crebier, "Power electronic converter emc analysis through state variable approach techniques," *IEEE Transactions on Electromagnetic Compatibility*, Vol. 43, No. 2, 229–238, May 2001.
16. Labarre, C., F. Costa, and C. Gautier, "Wiener filtering applied to magnetic near field scanning," *Progress In Electromagnetics Research*, Vol. 96, 63–82, 2009.